A Michelson interferometer for seismic wave measurement: theoretical analysis and system performances

Fausto Acernese[a,b], Rosario De Rosa[b,c], Fabio Garufi[b,c], Rocco Romano[a,b] and Fabrizio Barone[a,b]

[a] Dipartimento di Scienze Farmaceutiche, Università degli Studi di Salerno, Via Ponte Don Melillo, I-84084 Fisciano (SA), Italia

[b] INFN Sezione di Napoli, Complesso Universitario di Monte S. Angelo Via Cintia, I-80126 Napoli, Italia

[c] Dipartimento di Scienze Fisiche, Università degli Studi di Napoli Federico II, Complesso Universitario di Monte S.Angelo, Via Cintia, I-80126 Napoli, Italia

ABSTRACT

This papers describes a new low-frequency seismic sensor for geophysical applications. The instrument is basically a monolithic tunable folded pendulum with an interferometric readout system, that can be configured as seismometer or as accelerometer. The monolithic mechanical design and the introduction of a laser interferometric technique for the readout implementation make it a very sensitive and compact instrument with a very good immunity to environmental noises. Preliminary tests on the mechanical performances of the monolithic structure and on the optical reaodut have been performed. Interesting result is the measured resonant frequency of the instrument of $\approx 150\,mHz$ obtained with a rough tuning, demonstrating the feasibility of a resonant frequency of the order of $5\,mHz$ with a more refined tuning. The mechanics of the seismic sensor, the optical scheme of the readout system, the theoretical predictions and the preliminary experimental performances as seismometer are discussed in detail, together with the foreseen further improvements.

Keywords: Seismometer, Accelerometer, Michelson Interferometer, Folded Pendulum

1. INTRODUCTION

The development of low-noise high-resolution seismic sensors covering the seismic signal band from milliHertz to decaHertz has been quite slow in the last decades. Although many portable, efficient and robust seismic sensors have been developed in these last decades and many new ideas and techniques are being exploited, no one has improved the characteristics of band and sensitivity of the cornerstone sensor of the Global Seismographic Network (GSN), the Streckeisen STS-1, that is aging and no longer in production. This is probably due to the fact that the researchers in the field believe that the development of a sensor spanning the frequency band from millihertz to decahertz, like STS-1, is not technically convenient for many reasons, but that it is preferable to develop separate sensors to cover the whole frequency band. On the other hand, also industry shows little interest in developing a substitute sensor for the STS-1, probably due to unfavourable returns of the investments. Actually, the idea of using separate sensors covering different bands is not only related to technical difficulties, but it arises from a traditional distinction of seismic waves from signal analysis point of view (see Table 1). In fact, travelling waves from earthquakes are divided into three categories depending upon the source-receiver distance while the Earth's free oscillations, or normal modes, form another category. Earth's free oscillations have particular importance for long-period seismometry, because they are observed following large earthquakes as spectral peaks in the frequency band of $0.3 \div 7\,mHz$. The gravest mode of vibration, $0S2$, has a frequency of $0.3\,mHz$, and a splitting of this peak is frequently observed. At higher frequencies, the split modes overlap, and the spectral resolution decreases. Above $\approx 7\,mHz$, normal modes are too closely spaced to be resolvable, and other techniques, based on propagating wave theory, are used for the analysis of seismograms. Therefore, from what pointed above, there is a clear scientific need of seismic sensors very sensitive and with band extended towards the low frequency part of the seismic spectrum.

Send correspondence to Prof. Fabrizio Barone - E-mail: fabrizio.barone@na.infn.it

Remote Sensing for Environmental Monitoring, GIS Applications, and Geoloy VI, edited by Manfred Ehlers, Ulrich Michel, Proc. of SPIE Vol.6366, 63660I, (2006) - 0277-786X/06/$15 - doi: 10.1117/12.687907

Category	Distance	Frequencies	RMS Amplitudes
Local Signals	up to $\approx 30\,km$	$0.3 \div 30\,Hz$	to $\approx 10\ \ m/s^2$
Regional Signals	$\approx 1000\,km$	$10^{-1} \div 10\,Hz$	to $\approx 10^{-1}\,m/s^2$
Teleseismic	$\approx 10,000\,km$	$10^{-2} \div\ \ 1\,Hz$	to $\approx 10^{-3} m/s^2$
Normal Modes	Whole Earth	$10^{-4} \div 10^{-2}\,Hz$	to $\approx 10^{-5}\,m/s^2$

Table 1. Classification of the seismic signals

The techniques used for seismic sensors development are well known, so that we synthetise here only some important points. In a classic seismometer, the output signal is proportional to the displacement (or velocity) of the test mass due to the inertial force generated by seismic ground motion. Actually, this technique is nowadays used only in short-period seismometers, while broadband seismometers generally use a force-feedback design (accelerometers), which largely improves the linearity of the sensor, but reducing its dynamic range. In these instruments the inertial force is compensated by a feedback force, generated with a suitable control system and applied to the test mass using an electromagnetic transducer. Of course, although this technique clearly limits the sensor measurement band, due to the introduction of stability problems related to the control loops, it has the great advantage that the feedback force generated is proportional to the ground acceleration, and, therefore, the current used to drive the transducer coil is directly proportional to the ground acceleration, too. Although technology has largely improved in these years, nevertheless all the new designs of seismic sensors had to face the important and common problems to all the sensors: dynamic range, stability and noise floor, the latter due in particular to the Brownian motion of the suspended mass (thermal noise). The conclusion is that years of experiments and tests on seismic sensors have demonstrated that it is a very difficult task to improve or simply to reach the noise floor of the STS-1 sensor. Anyway many technologies have been proposed for seismic sensors design, many of them very promising. Here we quote only some of the sensors already developed: electrochemical transducer suspensions, squid displacement sensors, magnetic levitation seismometers, ferro-fluid suspensions, superconducting gravimeters, etc.

Among the possible and available techniques, developed in the past and available in literature and/or currently used in experiments of physics or in commercial instruments, we chose the Folded Pendulum technique. Folded Pendula, called also *Watt-linkage*, are classical suspension systems developed in 1962,[1] but recently ridescovered and developed again for application in gravitational wave research as ultra-low frequency pendulum resonators for vibration isolation in interferometric detectors of gravitational waves.[2] Actually these systems were too large to be used as instrumentation to be placed in a limited space or to be used as sensor in large and distribuited networks, because of a required compromise between the residual elasticity and the suspended load. More recently single-axis monolithic accelerometers have been developed to be used as sensors in the control system of advanced seismic attenuators. In fact, the progress in precision micro-machining has allowed the construction of extremely soft flexures at the pendulum's hinges, so that it has been possible to build a broadband single-axis monolithic Folded Pendulum of reasonable size with natural frequencies $< 1Hz$ to be used as sensor for the automatic control of advanced seismic attenuation systems.[3] These monolithic sensors exhibit very good performances, as we tested in our Laboratories of Salerno and Napoli, but have also a large margin of improvement both in sensitivity and in band. Using this valuable know-how we developed a new seismic sensor, aiming to a low-noise high-resolution seismic sensor oriented towards the low frequency band of the seismic spectrum for geophysical applications, both as a stand-alone sensor or as part of large and geographically distributed seismic networks. Our design is funded on two main cornerstones. The first one is the foreseen further technological improvement of micro-machining techniques, that will largely help us in reducing the sensor size to dimensions suitable for placing it in seafloors or in boreholes. The second cornerstone is the use of laser interferometric techniques for the implementation of the sensor readout system, that will improve its sensitivity together with its immunity to environmental noises. These interferometric techniques have already been successfully used by our group for the implementation of interferometric velocimeters.[4]

On the basis of what discussed above, we decided to move along three different directions for the development of a low-noise high-sensitivity sensor: 1) mechanics (optimization of the sensor mechanical performances); 2) optics (improvement of the sensitivity and noise immunity of the readout system); 3) electronics (design of an ad-hoc control and acquisition system well integrated with the sensor mechanics and optics).

In the following sections we will describe the status of the seismic sensor and its mechanical and optical performances. In particular, we report and discuss the expected best theoretical performances in connection with the experimental measurements. Finally, we describe the next planned steps necessary to improve the system and reach the design sensitivity.

2. SEISMIC SENSOR MECHANICAL MODEL

An accurate description of the dynamics of a Folded Pendulum (hereafter FP) is given by the simplified Lagrangian model developed by J. Liu et al.,[5] based on the mechanical scheme shown in Figure 1. The FP Model consists of two vertical beams of lengths l_1 and l_2 and masses m_{a_1} and m_{a_2}, respectively. The central mass is modeled with two equivalent masses, m_{p_1} and m_{p_2}, located near the hinge points at distances l_{p_1} and l_{p_2} with respect to the pivot points of the pendulum arm and of the hinging point of the oscillating mass.

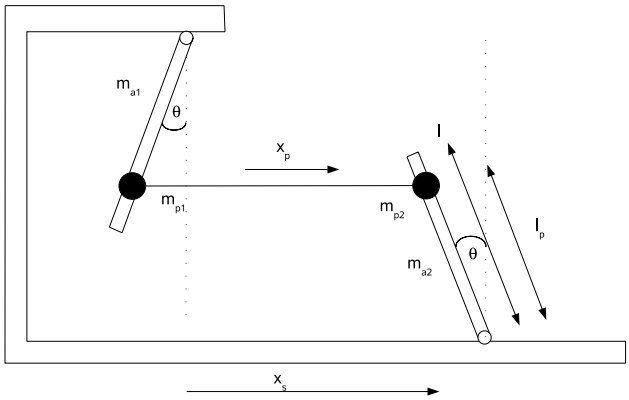

Figure 1. Folded Pendulum Mechanical Model

Assuming that the centre of mass of the pendulum is in $l/2$ and using the approximation of small deflection angles, then potential energy is given by:

$$U = \frac{1}{2}\left(\frac{m_{a_1}gl_1}{2} - \frac{m_{a_2}gl_2}{2} + m_{p_1}gl_{p_1} - m_{p_2}gl_{p_2} + k\right)\theta^2 = \frac{1}{2}\mathcal{K}_{eq}\theta^2 \tag{1}$$

where θ is the angle of deflection and k is the cumulative angular stiffness of the joints. As it will be clear in the following sections, these assumptions are well justified and fulfilled by the implementation of the FP sensor prototype.

Equation 1 shows that the FP potential energy can be considered as the combination of two potential energies: the potential energy of a simple pendulum and the potential energy of an inverted pendulum. The advantage of using a FP mechanical architecture becomes clear by plotting Equation 1: the coupling between a simple pendulum and an inverted pendulum allows the implementation of an oscillating system whose stiffness can be virtually reduced to very low values or cancelled, provided that the stability condition is preserved. In Figure 2 the typical shapes of the potential energy functions for a Pendulum, for an Inverted Pendulum and for a Folded Pendulum are reported for comparison.

The mechanical characteristics of a FP can be changed in different ways. Here we describe the technique we developed for tuning the FP resonant frequency and for choosing the shape of the potential energy, both operations necessary for the experimental setting of the FP sensor transfer function. In fact, Equation 1 shows that it is possible to change the shape of the potential energy, by changing the values of the masses m_{p_1} and

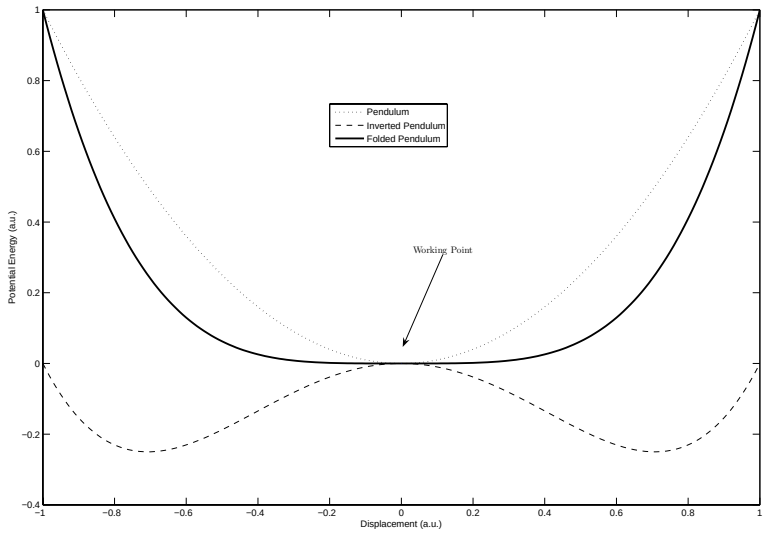

Figure 2. Potential Energy of a Pendulum, of an Inverted Pendulum and of a Folded Pendulum

m_{p_2}. These values can be changed by adding an external mass (tuning mass), M_l, placing it at a distance D from the pendulum suspension point. Defining S as the distance between the FP hinges points, then the values of the masses m_{p_1} and m_{p_2} change according to the relations

$$\begin{aligned} m_{p_{1_{new}}} &= m_{p_{1_{old}}} + M_l \left(1 - \frac{D}{S}\right) \\ m_{p_{2_{new}}} &= m_{p_{2_{old}}} + M_l \left(\frac{D}{S}\right) \end{aligned} \tag{2}$$

Therefore, the new values of the masses m_{p_1} and m_{p_2} change the value of the equivalent stiffness $\mathcal{K}_{eq}$, and, as consequence, the value of the FP resonant frequency. Hence, as a conclusion, the FP resonant frequency can be easily modified by changing the value, M_l, and the position, D, of a tuning mass as shown in Figure 3, where the FP resonant frequency is plotted as function of the value and position of the tuning mass. The frequency plateau shows the FP instability region.

The FP Transfer Function can be easily obtained by solving the Lagrange Equations. Defining the quantities x_s, the coordinate of the pendulum frame (fixed to the ground), and x_p, the coordinate of the FP mass (see Figure 1), then the FP transfer function is

$$\frac{x_p}{x_s} = \frac{\omega_0^2 - A_c\omega^2}{\omega_0^2 - \omega^2} = 1 + \frac{(1 - A_c)\omega^2}{\omega_0^2 - \omega^2} \tag{3}$$

where

$$\omega_0^2 = \left(\frac{g}{l_p}\right) \cdot \frac{(m_{a_1} - m_{a_2})\frac{l}{2l_p} + (m_{p_1} - m_{p_2}) + \frac{k}{gl_p}}{(m_{a_1} + m_{a_2})\frac{l^2}{3l_p^2} + (m_{p_1} - m_{p_2})} \tag{4}$$

is the square of FP resonant angular frequency and

$$A_c = \frac{\left(\frac{l}{3l_p}\right)(m_{a_1} - m_{a_2})}{(m_{a_1} - m_{a_2})\frac{l^2}{3l_p} + (m_{p_1} + m_{p_2})} \tag{5}$$

is the parameter related to the centre of percussion effects.[5] The structure of these two equations allows the definition of a FP equivalent mass as

$$M_e = (m_{a_1} - m_{a_2})\frac{l^2}{3l_p} + (m_{p_1} + m_{p_2}) \tag{6}$$

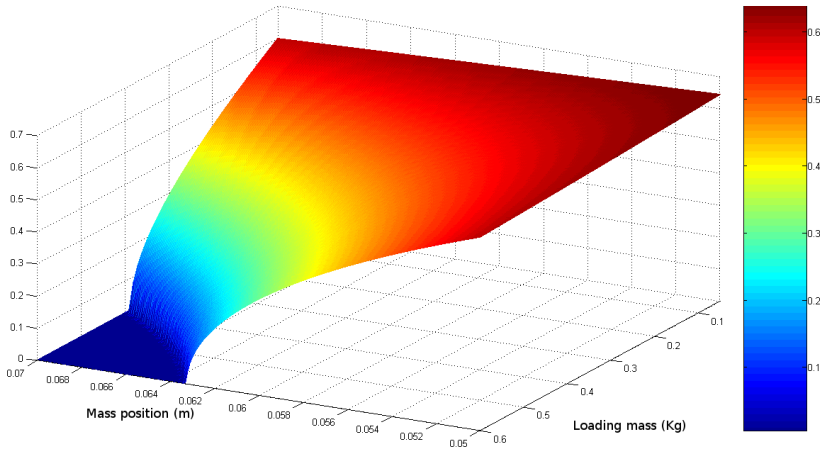

Figure 3. Folded Pendulum Resonant Frequency Tuning Technique

Finally, the mass displacement transfer function, that is the transfer function of the seismic sensor used as seismometer, can be obtained by rearranging Equation 3

$$\frac{x_p - x_s}{x_s} = \frac{(1 - A_c)\omega^2}{\omega_0^2 - \omega^2} \tag{7}$$

As we will show in the following sections, this analytical model well fits the experimental data and, at this level of development of the FP seismic sensor, is adequate for a good description and interpretation of the experimental results. Of course, we already found differences among the experimental evidence and the theoretical predictions. The most important difference is the lack of prediction of the Q of the mechanical system, since Equation 3 describes an ideal FP mechanical sensor. For this task it would have been necessary the use of a Lagrangian Dissipative Model for taking into account two important physical effects: the effect of the air on the pendulum motion and the effects of energy dissipation in the hinges of the mechanical pendulum. Actually, these effects are quite difficult to quantify analytically, so that we preferred to introduce an empirical dissipative term in the transfer fucntion based on the measured Q. Anyway, at the same time, since we expect that further improvements of the FP sensor mechanics necessary to reach its design sensitivity cannot be based anymore on a pure analytical model, we started a series of numerical simulations of the full FP mechanical system using methods based on finite element analysis.

3. SEISMIC SENSOR PROTOTYPE IMPLEMENTATION

The implementation of a first prototype of FP seismic sensor has required the choice of suitable technological solutions necessary to guarantee good sensitivity, directivity, long term stability, low coupling effects with environmental noises, small dimensions and robustness. In this section we describe in detail the two basic points of the FP sensor prototype: the mechanical structure and the optical readout system.

3.1. Folded Pendulum mechanical implementation

The structure of our FP mechanical prototype is monolithic, obtained using precision micro-machining techniques. The advantages of this choice is clear. In fact, a monolithic structure allows to maintain the Q-factor of the material and its characterisitcs of thermal sensitivity, while in a non monolithic structure shear effects at the contact surface between separated mechanical parts can generate hysteresis and dissipation. Furthermore, the directivity of the sensor can be largely improved with a careful mechanical design. It has been demonstrated that coupling factors of less than 10^{-4} among the different degrees of freedom have been obtained in monolithic structures.[3]

We have analyzed many materials for the FP implementation, with particular attention to Aluminium and Copper-Berillium, which were very good candidates. Finally we decided to use the aluminium alloy 7075-T6 for the first prototypes. The reasons of our choice are mainly due to the fact that, beyond the good thermal conductivity, the immunity to electromagnetic field, the high strength and low friction characteristics, the aluminium is a material not expensive and its machining is relatively easy and cheap. The latter characteristics are very important in a prototyping phase.

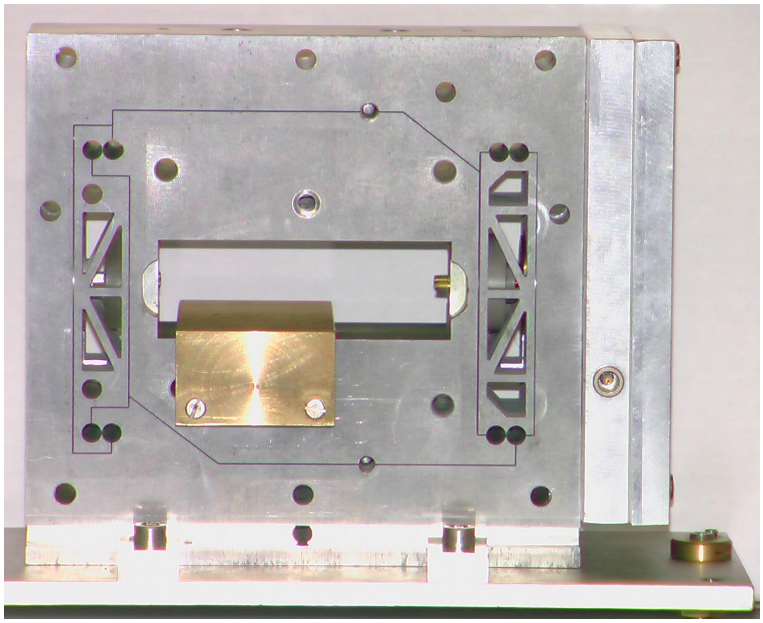

Figure 4. Picture of the Folded Pendulum Sensor we tested as Seismometer Prototype. On the sensor left side there is the pendulum mounting of the mirror for the optical read-out system. On the sensor right side, mounted on the inverted pendulum, there is a prototype of the coil-magnet actuation system for the implementation of the FP control when used as an accelerometer.

A picture of the FP mechanical sensor is shown in figure 4. The FP was obtained by machining a $140 \times 134 \times 40\,mm$ bulk of metal. A thin $250\,\mu m$ wire cut is used to separate the pendulum arm, the inverted pendulum arm and the central mass, from the frame. The four torsional flexures, connecting the pendulum arms to the central mass and to the frame, are circular notch fringes $50\,\mu m$ thick. The arms are $71.5\,mm$ long, spaced by $102\,mm$. The masses of the pendulum arm, of the inverted pendulum arm and of the test mass are $m_{a_1} = 41.7\,g$, $m_{a_2} = 49.6\,g$ and $(m_{p_1} + m_{p_2}) = 753.5\,g$ respectively. The total mass of the mechanical part is $1710\,g$. Note that both the FP arms have suitable designed openings necessary to reduce their masses and moment of inertia, without reducing their rigidity and simmetry. A central opening is made in the test mass in order to introduce a tuning mass of $336\,g$ for a fine tuning the FP resonant frequency. Finally, the sensor has been positioned on platform for its levelling.

The most critical part of the seismometer are the four flex joints which support the test mass. Each joint is a circular notch hinge that can be modelled using the Tseytlin formula.[6] In this approximation the angular stiffness can be calculated as:

$$k = \frac{Eat^2}{16[1 + \sqrt{1 + 0.215(2R/t)}} \tag{8}$$

where a is the sum of the width of all the joints, t is the thickness at the centre, R is the radius of curvature and E is the Young's modulus of the material. In the joints the total stress can be divided in tensile stress σ_T and bending stress σ_B. Calculating this values using the parameter of developed seismometer we obtained $\sigma_T \leq 10\,MPa$ and $\sigma_B \leq 60\,MPa$. These values show that we are very far from the $550\,MPa$ of the material's elastic limit, that ensures the robustness and the long-term durability of the mechanics.

3.2. Optical Readout Implementation

The readout system of the sensor is optical, based on laser interferometry. This solution guarantees a very high readout sensitivity toghether with very low coupling effects with environmental noises. The optical scheme is shown in Figure 5. From this figure it is easy to see that the optical readout system is basically a combination of an optical lever and a classic Michelson interferometer.

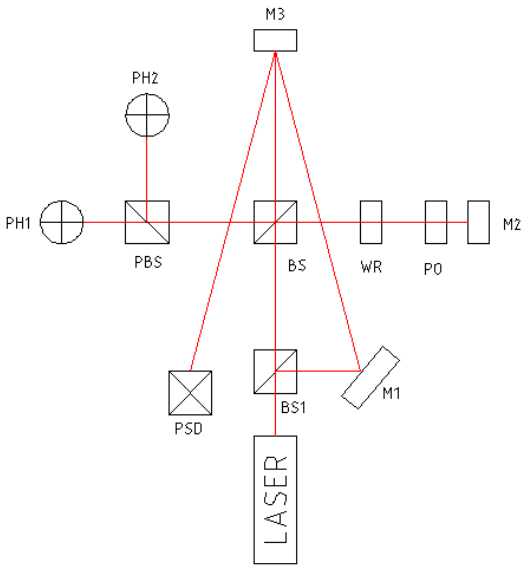

Figure 5. Optical scheme of the implemented readout system.

The optical readout works in a very simple way. A stabilised laser beam ($\lambda = 632.8\,nm$, $P = 3mW$) is divided into two beams by the beam splitter $BS1$. The first beam is used for the implementation of the Optical Lever to obtain a general purpose signal proportional to the relative motion of the test mass with respect to the sensor frame. This signal is used as output signal when the sensor is used as seismometer. The second beam, instead, is used for the implementation of a quadrature Michelson interferometer, whose goal is that of providing a very precise error signal describing the motion of the test mass with respect to the frame. This signal is the output signal when the sensor is used as force feedback accelerometer and the error signal for the control system. In this latter case, the closed loop strategy is divided into two sequential steps:

1. The optical lever provides the error signal for the FP control. Considering the displacement sensitivity of the optical lever, discussed in the next session, it is possible to reduce the movement of the mirror M3, attached to the intertial mass of the FP, within an interferometric fringe.
2. The interferometric signal is used then as error signal for the control. In this phase the sensitivity of the Michelson interferometer, better of the optical lever, provides a more accurate error signal, and allows the locking the test mass on the frame. Therefore the error signal, that is the acceleration signal, is the signal sent to the coil-magnet actuator.

Of course, when the sensor is used ad force feedback accelerometer there is the need of an actuator, that in our case is a coil-magnet actuator mounted on the inverted pendulum arm (see Figure 4).

The optical scheme shown in Figure 5 can be easily described. In the Optical Lever, the laser beam, divided by the beam splitter BS1 and reflected by the mirror M1, impinges on the mirror M3 attached to the lateral side of the sensor test mass, which reflects it to the Position Sensor Detector (PSD S2044 by Hamamatsu©). Therefore, the signal from the PSD, properly processed, provides a signal proportional to the mirror M3 displacement, limited only by the photodiode shot-noise. In the quadrature Michelson interferometer, the laser beam is first

divided by the beam splitter BS1. In our scheme the laser is oriented in such a way that the polarisation axis is rotated of $\pi/4$ radians with respect to the alignment of the beam splitter BS and reference mirror M2. The polarised beam oriented at this angle is vectorially equivalent to two beams of equal intensity, one polarised vertically and one polarised horizontally. The two beams are finally divided using a polarised beam splitter (PBS) and a photodiode for each beam, PH1 and PH2. A polarised device called 1/4 wave retarder (WR), designed to slow light polarised along its axis more than the light polarised perpendicularly to its axis. Its axis is placed in parallel to the vertical polarisation of beam, effectively adding 1/4 wavelength of its path. The photodiodes outputs will always differ by 1/4 of a fringe, or $\pi/2$ from each other, so that the beams in the two arms are in quadrature. Therefore using a phase-unwrapping technique it is possible to reconstruct the mirror displacement.

4. SENSITIVITY CURVE

In this section we model and evaluate the theoretical limits of the FP sensor, building a sensitivity curve describing the best performances achievable with our FP sensor. The discussion is limited to the performances obtainable as seismometer, that is the FP sensor in open loop configuration. This is due to the fact that up to now we made only tests on the FP sensor as seismometer.

There are three different main instrumental noise limiting the sensitivity of the FP sensor in seismometer configuration: mechanical noise, optical noise and electronics noise. In the following we analyze these noises and build the best theoretical sensitivity curve.

4.1. Mechanical Noise

Let us consider the Hooke law with dissipative force as

$$F_{elest} = -K[1 + \phi(\omega)]\Delta x \tag{9}$$

where $\phi(\omega)$ is the loss angle. Therefore, for the internal thermal noise, the quality factor Q of the FP can be calculated as

$$Q = \frac{1}{\phi}\frac{M_e l_p^2 \omega_0^2}{k} \tag{10}$$

and it can be measured as

$$Q = \frac{n\pi}{\ln(x_k/x_{k+n})} \tag{11}$$

where x_k are the amplitudes of the impulse responce. The thermal noise can be then evaluated as

$$x_{th}(f) = \sqrt{\frac{4K_B T l_p^2}{\pi Q M_e k}\frac{f_0^4}{f^5}}\ \left[\frac{m}{\sqrt{Hz}}\right] \tag{12}$$

Using the equations 10 and 11 we obtained a measured quality factor $Q \approx 4$, whose value is very small compared to the theoretical one for Aluminium ($Q \approx 3000$). Having performed our tests in air, this reduction is easily attributed to the presence of air between the oscillating mass and the reference frame. If the seismometer were under vacuum $Q \to 3000$ as $P \to 10^{-4}\, mbar$.[3] In our evaluation of the thermal noise we use a factor $Q = 4$.

4.2. Optical Noise

The optical noise is related to the radiation pressure of the laser source and to the shot noise of the photodiodes. The radiation pressure can be modeled as

$$x_{rad} = \sqrt{\frac{hP_0}{8\pi^3 c\lambda M_e f^2}}\ \left[\frac{m}{\sqrt{Hz}}\right] \tag{13}$$

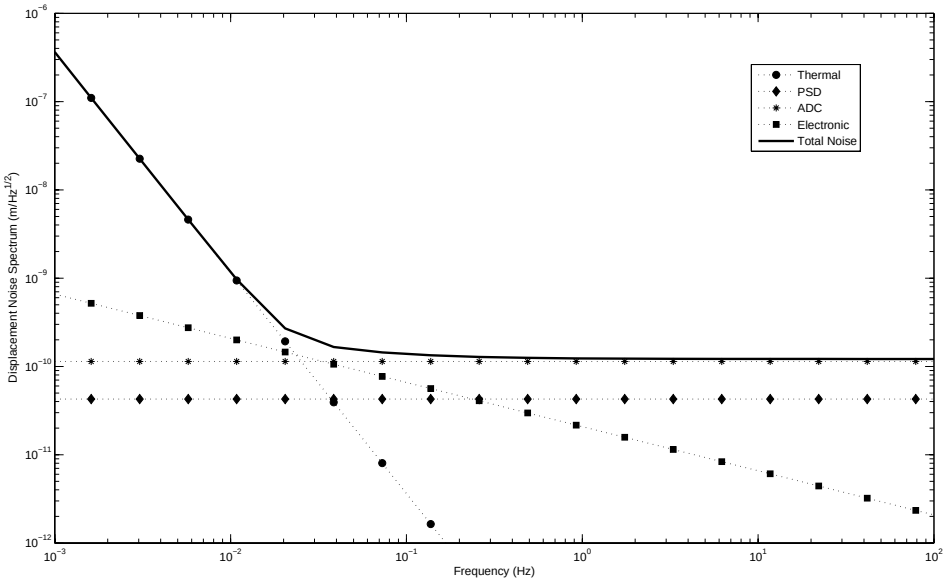

Figure 6. Total noise of the implemented open-loop seismometer

where h is the Planck constant, P_0 is the power of the laser source, c is the velocity of light, λ is the laser wavelength and M_e is the equivalent mass of the accelerometer. On the other hand, using the results of Barone et al.,[7] then the minimum detectable displacement due to the PSD shot noise is

$$x_{sh}(f) = \frac{L}{2}\sqrt{\frac{2hc}{\eta\lambda P_0}}\left[\frac{m}{\sqrt{Hz}}\right] \tag{14}$$

where L is the width of the PSD and η is the quantum efficiency of the PSD. A quick analysis of the order of magnitude of these two noise lead to the conclusion that in this case the radiation pressure noise of the light source is less relevant respect to the PSD shot noise, so that it can be neglected.

4.3. Electronics Noise

The Voltage-Current amplifiers used have been designed to minimise the electronic noise. The principal noise sources are: the Johnson noise of the resistors, the shot noise and he $1/f$ noise. Taking into account the parameters of the electronic components used in the amplifiers, the electronic noise can be model in equivalent mass displacement as

$$x_{el}(f) = \frac{\tilde{I}_n(f)}{|dI/dx|} = 4\cdot 10^{-10}\left(\frac{\tilde{I}_n(1\,mHz)}{1.7\cdot 10^{-10}}\right)\left(\frac{1\,mW}{P_0}\right)\left(\frac{1\,mHz}{f}\right)^{1/2}\left(\frac{L}{1\,mm}\right)\left[\frac{m}{\sqrt{Hz}}\right] \tag{15}$$

where $\tilde{I}_n$ is the current noise of the operational amplifiers. Concerning the ADC noise, we used a real 16 bit with a sampling frequency $F_s = 2\,kHz$ and range of $-10 \div 10\,V$. Therefore, we modeled the ADC noise as a white noise with equivalent displacement spectral density

$$x_{ADC}(f) = \mathcal{C}\frac{20}{2^{16}\sqrt{F_s}}\left[\frac{m}{\sqrt{Hz}}\right] \tag{16}$$

where $\mathcal{C} = 2^{16}\cdot 100\mu m/6V$ in a calibration constant.

We then combined all these main noise sources, obtaining the sensitivity of seismometer in open loop configuration. The results are shown in Figure 6. As a final result, we evaluated the integrated noise in the band $10^{-3} \div 10^2$, that resulted $\approx 5\,nm$.

5. EXPERIMENTAL RESULTS

The first two experiments performed on the seismometer were aimed to test the resonant frequency tuning technique and to test its global performances in a long-term measurement, in order to understand how far the FP seismic sensor prototype is from its theoretical sensitivity.

To experimentally test the FP Resonant Frequency Tuning Technique a tuning mass of $336\,g$ was placed in the central opening, as shown in Figure 4. The tuning mass has then been moved in small steps. For each step, the FP natural frequency and the quality factor has been measured, using the signals coming from the photodiode, acquired using a 16 bit ADC with a sampling frequency of $5000\,Hz$. The FP has been placed on an optical bench and an episensor Kinemetrix©, model FBA ES-T, has been fixed near the FP to compare the bench movement in order to validate the measures.

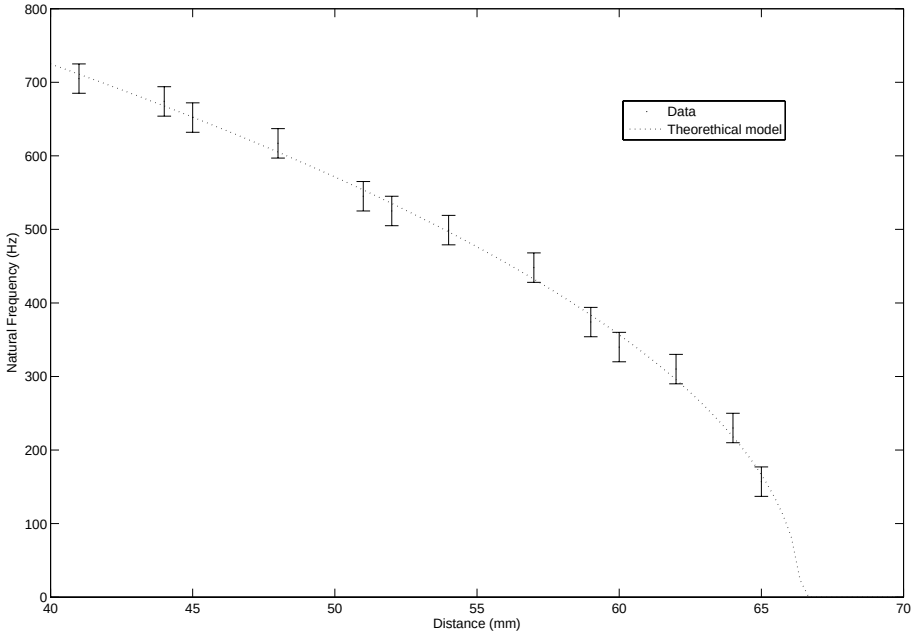

Figure 7. Folded Pendulum resonant frequency tuning: theoretical prediction and experimental data.

In Figure 7 the measured frequency with δf error bars versus the tuning mass position is shown. The data have been interpolated using equation 4 with adaptive parameters $(m_{p_1} + m_{p_2})$ and k. From this Figure is it clear that there is a good agreement between the data and the theoretical model. In Table 2 the interpolated parameters with an error bar with a level of significance $\alpha = 0.05$ are shown. Also in this case the distributed masses and the angular stiffness interpolated are in good agreement with the measured ones. The lower natural frequency measured is about $150\,mHz$. Note that, in this experimental setup, the position of the calibration mass has been fixed with a accuracy of about $\pm 1\,mm$.

Parameter	Interpolated Value with $\alpha = 0.05$	Measured Value
Central Mass	$778 \pm 45\,g$	$753\,g$
Angular Stiffness	0.077 ± 3	0.078

Table 2. Experimental and interpolated parameters

Considering Figure 7, we note that to furtherly decrease the natural frequency without reach the FP instability, it is necessary to improve the calibration procedure, refining the tuning mass positioning. This improvement is now under test by means of a piezoelectric system. On the basis of preliminary results we can state that with a resolution of $2\,\mu m$ a frequency of $5\,mHz$ can be in principle obtained.

Finally, in Figure 8 we report the first long term data acquisition from the seismometer compared with the expected sensitivity curve evaluated for the seismometer and with the standard High and Low Noise Peterson Model.[8] From this figure, although very preliminary, it is possible to see the very good potentialities of the FP sensor.

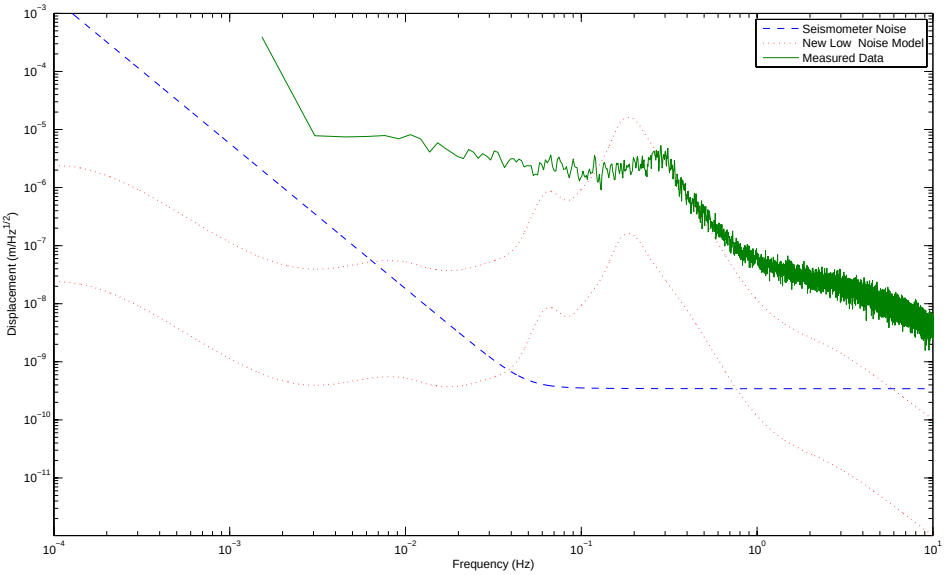

Figure 8. Preliminary Spectrum of the FP seismometer output compared with the High and Low Noise Peterson Model (filtered by the seismometer transfer function) and with the best expected sensitivity curve of the FP seismometer prototype.

6. CONCLUSIONS

In this paper we have described a new monolitich seismic sensor developed for geophysical applications, that can be used both as seismometer and force feedback accelerometer. Preliminary tests, performed only in its configuration as seismometer, are reported and discussed in this paper. Relevant is the preliminay result of a resonant frequency of 150 mHz and the possibility, to be experimentally demonstrated, of obtaining a resonant frequency of the order of 5 mHz with a suitable frequency tuning. A preliminary set of measurements have been reported and compared with the expected best sensitivity of the seismometer prototype, showing that large improvements of the FP sensor performances are possible. In the next months the FP sensor will be tested also as accelerometer and a campaign of measurements both for calibration and for defining further improvements is foreseen.

REFERENCES

1. E. S. Fergusson, *US Nat. Museum Bull.*, **228**, 185 (1962)
2. D. G. Blair et al., *Phys. Lett. A*, **193**, 223 (2004)
3. A. Bertolini et al., *Nucl. Instr. and Meth.*, **556**, 616 (2006)
4. F. Acernese, F. Barone, R. De Rosa, L. Milano, *Proc. SPIE: Remote Sensing for Environmental Monitoring, GIS Applications, and Geology IV*, **5574**, 299 (2005)
5. J. Liu, D. G. Blair, *Phys. Lett. A*, **228**, 243 (1997)
6. M. Y. Tseytlin, *Rev. Sci. Instrument*, **73**, 3363 (2002)
7. F. Barone et al., *Phys. Lett. A*, **193**, 15 (1994)
8. J. Peterson, *Open File Report 93-322*, Albuquerque, New Mexico (1993)